

# Frustrated structural instability in superconducting quasi-one-dimensional $K_2Cr_3As_3$

Keith M. Taddei,<sup>1,\*</sup> Guangzong Xing,<sup>2</sup> Jifeng Sun,<sup>2</sup> Yuhao Fu,<sup>2</sup> Yuwei Li,<sup>2</sup>  
Qiang Zheng,<sup>3</sup> Athena S. Sefat,<sup>3</sup> David J. Singh,<sup>2,†</sup> and Clarina de la Cruz<sup>1</sup>

<sup>1</sup>*Neutron Scattering Division, Oak Ridge National Laboratory, Oak Ridge, TN 37831*

<sup>2</sup>*Department of Physics and Astronomy, University of Missouri, Missouri 65211, USA*

<sup>3</sup>*Materials Science and Technology Division, Oak Ridge National Laboratory, Oak Ridge, TN 37831*

(Dated: September 3, 2022)

We present neutron total scattering and density functional theory studies on quasi-one-dimensional superconducting  $K_2Cr_3As_3$  revealing a frustrated structural instability. Our first principles calculations find a significant phonon instability which, under energy minimization, corresponds to a frustrated orthorhombic distortion. In diffraction studies we find large and temperature independent atomic displacement parameters which pair distribution analyses confirms and shows as resulting from highly localized orthorhombic distortions of the CrAs sublattice and coupled K displacements. These results suggest a far more complex phase diagram than previously assumed for this unusual superconductor with the likelihood of subtle interplays of structure, electron-phonon and magnetic interactions.

PACS numbers: 74.25.Dw, 74.62.Dh, 74.70.Xa, 61.05.fm

Bardeen, Schieffer and Cooper's seminal 1957 paper, laid out the framework for superconductivity via an unspecified attractive interaction between electrons [1]. While prior to their work this interaction had already been identified as phonon-electron coupling, in the long history of unconventional superconductors (UNSC) no such universal interaction is identified and different interactions may be involved in different materials[2–4]. Yet in most UNSC, clear candidates manifest, through a seeming quasi-universal proximity to ordering instabilities - such as magnetism, charge-ordering, structural distortions or, as is often the case, confounding combinations of these orders [5–9]. For the most widely studied families (e.g. cuprates, iron-based, heavy-Fermion), a vital tool has been the ability to tune through the instabilities via parameters such as pressure, charge-doping and strain. This allows for detailed study of how the suppressed orders interact with the superconducting state [7, 10, 11].

Recently, a new family of possible UNSC was discovered,  $A_2Cr_3As_3$  (with  $A = Na, K, Rb, Cs$ ), which has generated significant interest due to potentially exotic physics and provocative properties such as quasi-one-dimensionality (Q1D), non-centrosymmetry, Luttinger-Liquid like behavior and the transition-metal pnictide composition [12–18]. The main structural motif of CrAs double-walled sub-nano tubes is a fascinating contrast with the 2D transition metal planes of the cuprates and iron-based superconductors. However, also unlike its 2D brethren, the  $A_2Cr_3As_3$  materials have proven difficult to tune, chemical doping has proven challenging and internal/external pressure suppresses the superconducting transition ( $T_c$ ) but not completely - disallowing study of a non-superconducting relative [15, 19]. Furthermore, while probes measuring dynamic phenomena have revealed signatures of spin-fluctuations, no long-range or-

der analogous to the spin/charge density waves of the classic UNSC has been observed and initial findings of a possible spin-glass phase in the  $ACr_3As_3$  stoichiometry have given way to newer reports of robust superconductivity with no static magnetism [20–26]. In the absence of the often observed dome phase diagram or clear evidence of a nearby instability, the superconducting state in this system remains unresolved - with as divergent suggestions as spin-fluctuations and phonons as mediating superconductivity [20, 27].

Motivated by our first principles calculations, which show that the ideal hexagonal structure is structurally unstable, we revisit the structure of  $K_2Cr_3As_3$ . Starting with a careful analysis of the atomic displacement parameters (ADPs), where we observe an anomalous temperature dependence. Using neutron total scattering techniques we find the anomalous ADP behavior localized to the  $ab$  plane and well modeled by an orthorhombic distortion nominally driven by a distortion of the CrAs tubes and a coupled displacement of the neighboring K sites. Our density functional theory calculations show a significant in-plane phonon instability but with a high degree of degeneracy. These results indicate that, in addition to the previously reported nearness to a magnetic instability,  $K_2Cr_3As_3$  has a structural instability albeit frustrated.

Neutron total scattering measurements were performed on the NOMAD time-of-flight diffractometer of Oak Ridge National Laboratory's Spallation Neutron Source and reduced using the instrument developed software [28, 29]. NOMAD detects neutrons diffracted over a wide range of scattering vectors ( $Q$ ) - including high  $Q$  where the Bragg condition is especially sensitive to the coherence of the nuclear structure (see supplemental material 30). The diffraction data were used (along with the data reported in Ref. 20) for Rietveld refinements (as

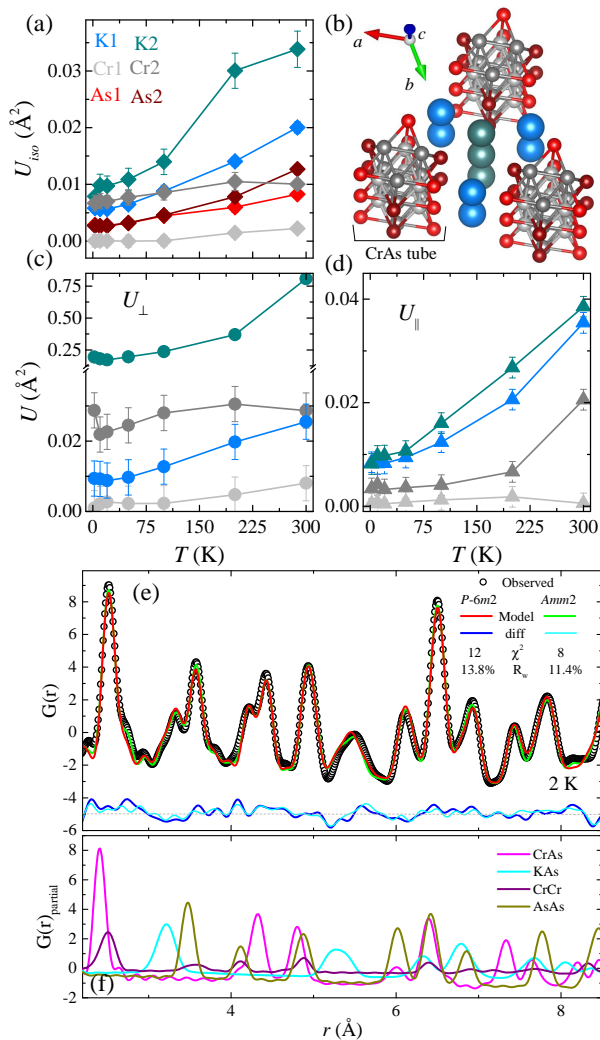


FIG. 1. Temperature dependence of  $\text{K}_2\text{Cr}_3\text{As}_3$  atomic displacement parameters ( $U$ ), from standard diffraction treatment (a).  $\text{K}_2\text{Cr}_3\text{As}_3$  structure showing triangular coordination of K2 site (b). Anisotropic  $U$  parameter determined from pair distribution function analysis for  $ab$  plane ( $U_{\perp}$ ) (c) and lattice  $c$  direction ( $U_{\parallel}$ ) (d). Fit of PDF data using the averaged  $P\bar{6}m2$  and distorted  $Amm2$  structure symmetry constraints (e). Partial PDF showing the K-As, Cr-As, Cr-Cr and As-As correlation functions for  $P\bar{6}m2$  fit (f).

implemented in the GSAS and EXPGUI software suites [31, 32]. The availability of high  $Q$  data allowed for reliable refinements of the ADP's (*i.e.* the mean square of the variance in atomic positions) which are sensitive to local (temporal or spatial) distortions [33–36].

Figure 1(a) shows the temperature dependence of the isotropic ADP's for each unique crystallographic site in  $\text{K}_2\text{Cr}_3\text{As}_3$ . We cautiously note that our ADP's are significantly larger than in the structurally related (and stable) Q1D Chevrel phases, than reported in the iron-based superconducting materials and similar in magnitude (for the K sites) to Einstein 'rattler' behavior seen in some

thermoelectric materials [36–39]. To this latter comparison, we similarly observe significant residual ADP at 2 K on the K1 and (more-so) K2 site while the Cr2 site not only exhibits a relatively large  $U_{iso}(T \rightarrow 0 \text{ K})$  but also shows little temperature dependence over the measured range. In contrast, the As1, As2 and Cr2 sites show Debye-Waller type behavior, tending towards low values as  $T \rightarrow 0 \text{ K}$ . The temperature dependence of the former three sites, indicates ADP's not exclusively driven by standard thermal effects and possible disorder or dynamic correlations on these sites.

$\text{K}_2\text{Cr}_3\text{As}_3$  can be defined as two species of alternating stacked planes each with a unique K, Cr and As site. The sets of K1,Cr1,As2 and K2,Cr2,As1 compose the  $z = 0, \frac{1}{2}$  planes respectively. An important element of the  $P\bar{6}m2$  structure is the non-centrosymmetry of the CrAs tubes' point group [40]. This is caused by the inequivalency of the two layers' K sites - which leaves the  $z = 0$  plane with 3 K to the  $z = \frac{1}{2}$  plane's single K (Fig. 1(b)). In addition to placing the K2 site in a larger As cage, it is predicted to cause different electron counts on the two CrAs layers [14, 40]. Therefore, the large ADP's found for the K2 and Cr2 sites should be coupled - with a change in the Cr2 plaquette bonding and thus the symmetry of the charge distribution within the tube resulting in or from a displacement of the K2 site.

In standard diffraction analysis, information about short-range correlations or disorder is secondary to the averaged structure as the main fitting features are Bragg reflections. In reciprocal space, short-range behavior shows up as decoherence of the high  $Q$  peaks and as broad features which are obscured by profile and background parameters in typical Rietveld refinement. However, the Fourier transform of the normalized diffraction pattern into the real space pair distribution function (PDF)  $G(r)$ , shifts the features of the fit pattern to local atomic correlations. Therefore, where standard diffraction analysis gives the average crystallographic structure, PDF analysis reveals local behavior and allows for the local distortions to be quantified through least-squares fitting of the data in real space.

Figure 1(e) shows a least-squares fit (as implemented in PDFgui [41 and 42]) using all the symmetry constraints of the average  $P\bar{6}m2$  symmetry to the low- $r$  region of PDF data collected at 2 K (see SM for more details on fitting). We start with the reported structure to refine our discussion of the ADP's, which are more directly refined in  $G(r)$  as peak widths. We perform fitting over the low- $r$  range of 2.1 - 20 Å, which covers approximately the first two unit cells, to accentuate the weighting of local structure. Motivated by the co-planar arrangement of the atomic sites, we model the anisotropic ADP's with in-plane ( $U_{\perp}$ ) and out-of-plane ( $U_{\parallel}$ ) components.

The resulting temperature dependent ADP's are shown in Fig. 1(c) and (d). The anisotropic treatment reveals the large and temperature independent ADP be-

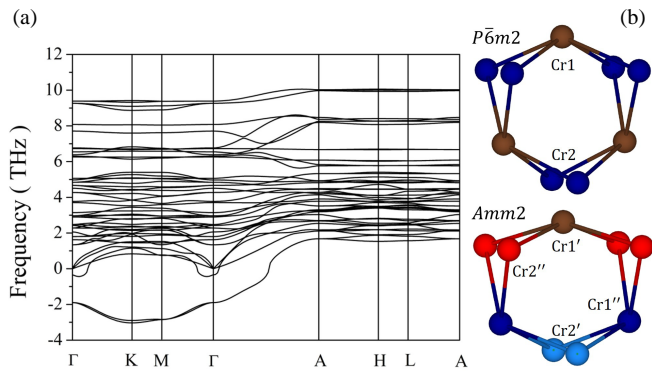


FIG. 2. Phonon dispersions for selected directions through the Brillouin zone (a). Fermi surface of  $K_2Cr_3As_3$  as calculated from density functional theory (b).

behavior of K2 and Cr2 respectively to arise from the in-plane components,  $U_{\parallel}$  is mostly Debye-Waller like. In both cases the  $U(T = 2\text{ K})$  values are quite large and indicate possible local disorder of the K2 and Cr2 sites within the  $ab$ -plane.

Density functional theory calculations were performed using the general gradient approximation, projector-augmented wave method and the general potential linearized augmented plane-wave method with the experimental lattice parameters (see SM)[20, 43–47]. The phonon dispersions are shown in Fig. 2(a). In contrast to previous reports, our calculations predict a substantial structural instability of the CrAs tubes as seen by the negative energy optical phonon branch along the in-plane  $\Gamma-K$ ,  $K-M$  and  $M-\Gamma$  directions [27]. While, the instability exhibits little in-plane dispersion, it is highly dispersive along  $\Gamma-A$  - corresponding to the CrAs tube direction. This indicates a tendency towards a structural distortion with little correlation between unit cells in-plane. This degeneracy represents a frustration that works against ordering

To study the resultant structural distortion we allowed the crystallographic parameters to relax following energy minimization. The obtained structure exhibits an  $Amm2$  orthorhombic distortion (Fig. 2(b)). The change to  $Amm2$  symmetry is a  $\Gamma$  point distortion, which - crucially - breaks the inversion axis perpendicular to the plane and splits the Cr1(2), As1(2) and K1 sites into 2 orbits. This reduces the Cr and As plaquettes'  $C_3$  symmetry to  $C_2$ . Additionally, it releases the symmetry constraints on the  $1c$  K2 site allowing for displacements along the  $(2,1,0)$  direction.

Quantitatively, this agrees with the anisotropic ADP parameters from our diffraction analysis. Noting the poor fit of the  $P\bar{6}m2$  model to the low- $r$  PDF data (Fig. 1(e)) and anomalous in-plane ADP's, we attempted modeling of our PDF data allowing for atomic displacements consistent with the  $Amm2$  spacegroup. As in

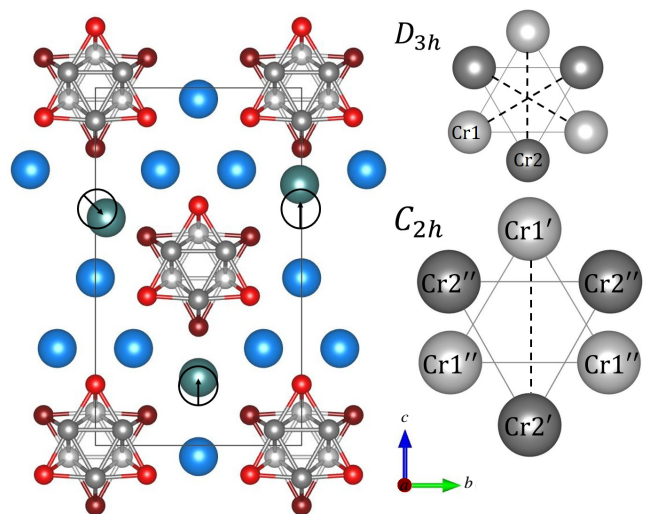


FIG. 3.  $Amm2$  structure determined in low- $r$  PDF fits, the results of the the three site K2 refinement are shown revealing a lack of displacement correlation between neighboring K2's (left). Symmetry of the Cr tubes in the  $P\bar{6}m2$  and  $Amm2$  space groups (point groups  $D_{3h}$  and  $C_{2h}$  respectively) with mirror plane represented by dashed lines (right).

the  $P\bar{6}m2$  refinements, the the atomic sites were refined within the symmetry constraints of the space group and parameters were handled to ensure the same number of refinable parameters in each model (see SM). As seen in Fig. 1(e) the  $Amm2$  model reduces the  $\chi^2$  and  $R_w$  parameters from 11.7 and 14.1% to 10.3 and 13.0% respectively. Moreover, the  $U_{\perp}$  for K2 is reduced from  $0.30\text{ \AA}^2$  to  $0.03\text{ \AA}^2$  (for first unit cell  $r$ -range). Both observations corroborate the predictions of our DFT work.

To further analyze this distortion, we look at the geometry of the CrAs tubes which is complicated by many similar bond lengths obscuring small distortions in  $G(r)$ . Nonetheless, a series of peaks ( $r = 2.6, 3.3$  and  $5.4\text{ \AA}$ ) can be identified which are poorly fit by the  $P\bar{6}m2$  model (Fig. 1(f)). Additionally, a general systematic over/under fitting of adjacent peaks is evident, which results from the anomalously large ADP of the K2 and Cr2 atomic sites (Fig. 1(e) and (f)). If fitting is performed using ADP values of similar materials and structures this trend is exacerbated revealing the large ADP's as a response to a series of over fit K-As and Cr-As correlation lengths - large ADP's cause broad peak shapes and are able to approximate small splittings or over fit peaks but cannot correct for under fit peaks in the model [37, 39]. If instead, the model is refined using  $Amm2$  symmetry constraints, the newly allowed in-plane displacement of the K2 site (as labeled in the original structure) alleviates the over/under count by shortening the K2 - CrAs tube spacing. In the  $Amm2$  model, the distortion of the K1 and Cr2 plaquettes, allows for a better fit of these split peaks. Collectively these changes result in a visually and

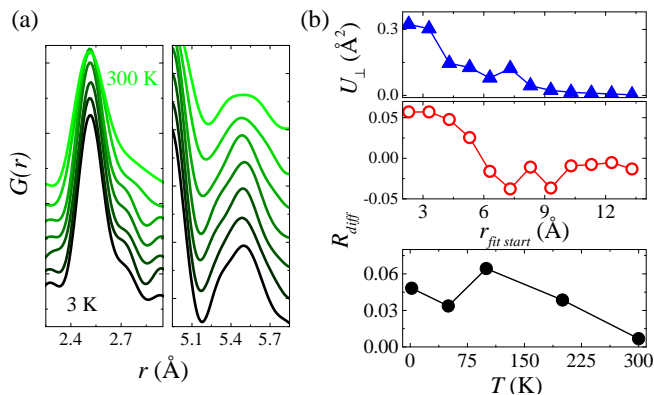


FIG. 4. Waterfall plots showing temperature dependence of the  $G(r)$  2.7 and 5.4 Å peaks (a).  $r$  dependence of refined in-plane ADP's and the normalized  $R$ -factors  $R_{diff}$  for boxcar (9 Å window) PDF fits using  $Amm2$  and  $P\bar{6}m2$  symmetry constraints as functions of starting  $r$  and  $T$  (b).

statistically better fit to the low- $r$   $G(r)$  data without the need for additional fit parameters.

The fit  $Amm2$  structure is shown in Fig. 3. The main differences from  $P\bar{6}m2$  (Fig. 1(b)) are a large displacement of the K2 site along the orthorhombic (2,1,0) direction and breaking of the CrAs tubes  $C_3$  rotational symmetry. The inequivalence of K count in the  $z = 0, \frac{1}{2}$  layers may reflect different bonding parameters in each layer [13, 21, 40]. Considering these results, one would expect the change of bonding in the Cr-Cr plaquettes to affect the electron distribution and so couple to the K position. In the case of a (2,1,0) K2 displacement, Cr-Cr(Cr-As) should decrease(increase) for the nearest Cr2 site. This is what we see, as the triply degenerate 2.66 Å Cr2-Cr2 bond breaks into a 2.55 and two 2.65 Å bonds and the Cr2-As1 bond of length 2.49 Å breaks into a 2.58 and two 2.51 Å bonds - the shorter(longer) corresponding to the Cr2 closest the displaced K.

The analysis of the standard diffraction and PDF data indicate that on the 1-2 unit cell (20 Å) scale there are significant local distortions but that they are uncorrelated over long distances, averaging to  $P\bar{6}m2$ . To investigate the scale of this transition, boxcar fits of the PDF data were performed by choosing a window size ( $\Delta r$ ) and then sliding the starting  $r$  value ( $r_{fitstart}$ ) of the fit range to increasing  $r$ . In this way, the analysis can be shifted from the local structure to the approximate averaged structure (high  $G(r)$  approximates the averaged structure as larger coordination spheres are invoked) and the relative goodness-of-fit of the different models can be investigated over different correlation lengths. To perform this analysis we utilized a  $\Delta r$  of 9 Å and shifted  $r_{fitstart}$  from 2.3 to 13.3 Å.

The normalized difference of  $R_w$  ( $R_{diff} = 2 * (R_{orth} - R_{hex}) / (R_{orth} + R_{hex})$ ) from boxcar fits is shown in Fig. 4(b). For the lowest  $r_{fitstart}$ , the orthorhombic

model results in significantly improved  $R_{diff}$ , however, by  $r_{fitstart} = 6.3$  Å the hexagonal model produces statistically identical  $R_w$  to the orthorhombic model - indicating that by 6.3 Å modeling with ADP's is as good as the orthorhombic distortion, with  $R_{diff}$  settling to zero for higher  $r_{fitstart}$ . Similarly, we can fit  $U_{\perp}$  as a function of  $r_{fitstart}$ , (Fig. 4(b)) revealing a quick drop-off of the abnormally large K2 ADP which approaches the value found from modeling  $S(Q)$  ( $U_{\perp} \approx 0.01$  Å<sup>2</sup>) by  $r_{fitstart} = 9$  Å.

These distance scales are approximately the size of the CrAs tubes but smaller than the intertube spacing and K2-K2 distance ( $\sim 10$  Å) indicating that the distortion is essentially uncorrelated between unit cells. We note that each CrAs tube has  $C_3$  rotational symmetry and therefore can 'choose' to distort along any of three directions. When  $r_{fitstart} = 6.3$  Å correlations over 15 Å are considered including the next nearest CrAs tube and 8 in-plane K2 correlations for every CrAs tube - that the fit is unimproved in the  $Amm2$  model indicates little to no correlation between unit cells. This is consistent with inherent frustration due to the  $C_3$ -axis and further indicated by the degeneracy of the relevant phonon mode in the  $k_z = 0$  plane. In fact, models using  $Pmm2$  symmetry which breaks the K2 site into two orbits and creates two distinct CrAs tubes, further reduces  $R_w$  however, the  $Pmm2$  symmetry produces more refinable parameters and direct comparisons of  $R_w$  with the  $P\bar{6}m2$  model are less unambiguous, we therefore base our conclusions on the  $Amm2$  distortion.

We performed PDF refinements with the symmetry constraints of the two K2 sites in the  $Amm2$  model removed, the resulting models reduced  $R_{diff}$  and resulted in uncorrelated displacements between the two sites (Fig. 3) which nonetheless remained along the mirror planes of the  $C_3$  symmetry. We suggest the distortion happen randomly from CrAs to CrAs tube, such disorder would give rise to the observed average structure and a large in-plane ADP for the K2 site.

Identifying whether these distortions are static or dynamic is of great interest to their possible relevance to superconductivity. However, the technique of time-of-flight neutron total scattering integrates over some finite energy transfer - inelastic signal will always be present meaning the instantaneous 'snap-shot' of the PDF pattern includes dynamic effects with the energy scale of several meV (or  $10^{-13}$  s) [48]. The temperature dependence of the distortion can also be used as an indirect probe for the time-scale of the correlations, with persistence to high temperatures being expected of more static effects. Figure 4(a) shows two of the clearest split peaks as a function of temperature. In both cases the distortion is seen to persist to 300 K - albeit with considerable broadening. As another test we performed fit comparison between the two models over the measured temperature range (Fig. 4(b)), despite a possible downturn at

300 K the orthorhombic model always produces reduced  $R$  factors. While we cannot determine definitively the time-scale of the distortion from our measurements, their temperature dependence is more indicative of a static distortion than of fluctuations. Further studies are needed to clarify this important distinction.

Our results indicate that  $\text{K}_2\text{Cr}_3\text{As}_3$  is susceptible to an orthorhombic distortion which is frustrated by its hexagonal symmetry. We find that the K2 site displaces along the  $Amm2$  symmetry modes towards one of its neighboring CrAs tubes and that there is a substantial distortion of the CrAs tube. However no significant correlation from unit cell to unit cell occurs. Our DFT calculations show that there is little in-plane  $k$  dependence to the unstable optical phonon mode agreeing with our local distortion model. Charge counting arguments suggest the motion of the K2 site and the distortion of the CrAs tube to be coupled. That  $\text{K}_2\text{Cr}_3\text{As}_3$  has such an instability is significant to the materials position within the wider family of UNSC as it more clearly places it on similar footing with these materials' which tend to exhibit structural and magnetic instabilities.

The part of the research that was conducted at ORNLs High Flux Isotope Reactor and Spallation Neutron Source was sponsored by the Scientific User Facilities Division, Office of Basic Energy Sciences, US Department of Energy. The research is partly supported by the U.S. Department of Energy (DOE), Office of Science, Basic Energy Sciences (BES), Materials Science and Engineering Division. The authors thank B.A. Frandsen, M. McDonnell and T.-M. Usher-Ditzian for guidance with PDFgui and J. Neufeind for help with data collection on NOMAD.

---

\* corresponding author taddeikm@ornl.gov

† corresponding author singhdj@missouri.edu

- [1] J. Bardeen, L. N. Cooper, and J. R. Schrieffer, *Physical Review* **108**, 1175 (1957).
- [2] J. Bardeen and D. Pines, *Phys. Rev.* **99**, 1140 (1955).
- [3] G. R. Stewart, *Advances in Physics* **66**, 75 (2017), <https://doi.org/10.1080/00018732.2017.1331615>.
- [4] M. R. Norman, *Science* **332**, 196 (2011).
- [5] D. Basov and A. Chubukov, *NATURE PHYSICS* **7**, 272 (2011).
- [6] S. Avci, O. Chmaissem, E. A. Goremychkin, S. Rosenkranz, J.-P. Castellán, D. Y. Chung, I. S. Todorov, J. A. Schlueter, H. Claus, M. G. Kanatzidis, A. Daoud-Aladine, D. Khalyavin, and R. Osborn, *Physical Review B* **83**, 172503 (2011).
- [7] A. Chubukov, *Annual Review of Condensed Matter Physics* **3**, 57 (2012), <https://doi.org/10.1146/annurev-conmatphys-020911-125055>.
- [8] R. M. Fernandes, a. V. Chubukov, and J. Schmalian, *Nature Physics* **10**, 97 (2014).
- [9] B. White, J. Thompson, and M. Maple, *Physica C: Superconductivity and its Applications* **514**, 246 (2015), superconducting Materials: Conventional, Unconventional and Undetermined.
- [10] P. Monthoux, D. Pines, and B. Lonzarich, *Nature* **450**, 1177 (2007).
- [11] S. Lederer, Y. Schattner, E. Berg, and S. A. Kivelson, *Proceedings of the National Academy of Sciences* **114**, 4905 (2017), <http://www.pnas.org/content/114/19/4905.full.pdf>.
- [12] J.-K. Bao, L. Li, Z.-T. Tang, Y. Liu, Y.-K. Li, H. Bai, C.-M. Feng, Z.-A. Xu, and G.-H. Cao, *Physical Review B* **91**, 180404 (2015), arXiv:arXiv:1412.0067.
- [13] P. Alemany and E. Canadell, *Inorganic Chemistry* **54**, 8029 (2015), pMID: 26230077, <http://dx.doi.org/10.1021/acs.inorgchem.5b01207>.
- [14] H. Jiang, G. Cao, and C. Cao, *SCIENTIFIC REPORTS* **5** (2015), 10.1038/srep16054.
- [15] Z. Wang, W. Yi, Q. Wu, V. A. Sidorov, J. Bao, Z. Tang, J. Guo, Y. Zhou, S. Zhang, H. Li, Y. Shi, X. Wu, L. Zhang, K. Yang, A. Li, G. Cao, J. Hu, L. Sun, and Z. Zhao, *SCIENTIFIC REPORTS* **6** (2016), 10.1038/srep37878.
- [16] Z. Yi, C. Chao, and Z. Fu-Chun, *Science Bulletin* **62**, 208 (2017).
- [17] M. D. Watson, Y. Feng, C. W. Nicholson, C. Monney, J. M. Riley, H. Iwasawa, K. Refson, V. Sacksteder, D. T. Adroja, J. Zhao, and M. Hoesch, *Phys. Rev. Lett.* **118**, 097002 (2017).
- [18] Q.-G. Mu, B.-B. Ruan, B.-J. Pan, T. Liu, J. Yu, K. Zhao, G.-F. Chen, and Z.-A. Ren, *Phys. Rev. Materials* **2**, 034803 (2018).
- [19] G. Cao, J.-K. Bao, Z.-T. Tang, Y. Liu, and H. Jiang, *Philosophical Magazine* **97**, 591 (2017).
- [20] K. M. Taddei, Q. Zheng, A. S. Sefat, and C. de la Cruz, *Phys. Rev. B* **96**, 180506 (2017).
- [21] H. Zhi, T. Imai, F. Ning, J.-K. Bao, and G.-H. Cao, *Physical Review Letters* **114**, 147004 (2015).
- [22] J. Yang, Z. T. Tang, G. H. Cao, and G.-q. Zheng, *Physical Review Letters* **115**, 147002 (2015).
- [23] H. Zhi, D. Lee, T. Imai, Z. Tang, Y. Liu, and G. Cao, *Physical Review B* **93**, 174508 (2016).
- [24] C. Cao, H. Jiang, X.-Y. Feng, and J. Dai, *Physical Review B* **92**, 235107 (2015).
- [25] Q.-G. Mu, B.-B. Ruan, B.-J. Pan, T. Liu, J. Yu, K. Zhao, G.-F. Chen, and Z.-A. Ren, *Phys. Rev. B* **96**, 140504 (2017).
- [26] T. Liu, Q.-G. Mu, B.-J. Pan, B.-B. R. J. Yu, K. Zhao, G.-F. Chen, and Z.-A. Ren, *Europhysics Letters* **120** (2018), 10.1209/0295-5075/120/27006.
- [27] A. Subedi, *Phys. Rev. B* **92**, 174501 (2015).
- [28] M. T. McDonnell, D. P. Olds, K. L. Page, J. C. Neufeind, M. G. Tucker, J. C. Bilheux, W. Zhou, and P. F. Peterson, *Acta Crystallographica Section A* **73**, a377 (2017).
- [29] J. Neufeind, M. Feygenson, J. Carruth, R. Hoffmann, and K. K. Chipley, *Nuclear Instruments and Methods in Physics Research Section B: Beam Interactions with Materials and Atoms* **287**, 68 (2012).
- [30] See Supplemental Material at.
- [31] B. H. Toby, *Powder Diffraction* **21**, 67 (2006).
- [32] A. Larson and R. Von Dreele, Report No. LAUR **Los Alamos National Laboratory, Los Alamos, NM**, 86 (2004).
- [33] D. W. J. Cruickshank, *Acta Crystallographica* **9**, 747 (1956).
- [34] J. Dunitz, V. Schomaker, and K. Trueblood,

- The Journal of Physical Chemistry **92**, 856 (1988), <https://doi.org/10.1021/j100315a002>.
- [35] B. Sales, B. Chakoumakos, D. Mandrus, and J. Sharp, Journal of Solid State Chemistry **146**, 528 (1999).
- [36] B. Sales, B. Chakoumakos, R. Jin, J. Thompson, and D. Mandrus, Phys. Rev. B **63**, 245113 (2001).
- [37] P. Gall, T. Guizouarn, M. Potel, and P. Gougeon, Journal of Solid State Chemistry **220**, 213 (2014).
- [38] B. C. Sales, B. C. Chakoumakos, and D. Mandrus, Phys. Rev. B **61**, 2475 (2000).
- [39] “Bafes2 crystal structure: Datasheet from “pauling file multinationals edition – 2012” in springermaterials,” (2006), copyright 2016 Springer-Verlag Berlin Heidelberg & Material Phases Data System (MPDS), Switzerland & National Institute for Materials Science (NIMS), Japan.
- [40] X.-X. Wu, C.-C. Le, J. Yuan, H. Fan, and J.-P. Hu, Chinese Physics Letters **32**, 057401 (2015).
- [41] C. Farrow, P. Juhas, J. Liu, D. Bryndin, E. Boin, J. Bloch, T. Proffen, and S. Billinge, Journal of Physics: Condensed Matter **19**, 335219 (2007).
- [42] T. Proffen and S. J. L. Billinge, Journal of Applied Crystallography **32**, 572.
- [43] J. P. Perdew, K. Burke, and M. Ernzerhof, Phys. Rev. Lett. **77**, 3865 (1996).
- [44] G. Kresse and D. Joubert, Phys. Rev. B **59**, 1758 (1999).
- [45] G. Kresse and J. Furthmüller, Phys. Rev. B **54**, 11169 (1996).
- [46] D. Singh and L. Nordström, *Planewaves, Pseudopotentials and the LAPW Method*, 2<sup>nd</sup> ed. ed. (Springer, Berlin, 2006).
- [47] A. Togo and I. Tanaka, Scripta Materialia **108**, 1 (2015).
- [48] B. A. Frandsen, K. M. Taddei, M. Yi, A. Frano, Z. Guguchia, R. Yu, Q. Si, D. E. Bugaris, R. Stadel, R. Osborn, S. Rosenkranz, O. Chmaissem, and R. J. Birgeneau, Phys. Rev. Lett. **119**, 187001 (2017).

**Supplemental Material for:  
Frustrated structural instability in superconducting quasi-one-dimensional  $K_2Cr_3As_3$**

Keith M. Taddei,<sup>1,\*</sup> Guangzong Xing,<sup>2</sup> Jifeng Sun,<sup>2</sup> Yuhao Fu,<sup>2</sup> Yuwei Li,<sup>2</sup>  
Qiang Zheng,<sup>3</sup> Athena S. Sefat,<sup>3</sup> David J. Singh,<sup>2,†</sup> and Clarina de la Cruz<sup>1</sup>

<sup>1</sup>*Neutron Scattering Division, Oak Ridge National Laboratory, Oak Ridge, TN 37831*

<sup>2</sup>*Department of Physics and Astronomy, University of Missouri, Missouri 65211, USA*

<sup>3</sup>*Materials Science and Technology Division, Oak Ridge National Laboratory, Oak Ridge, TN 37831*

(Dated: September 3, 2022)

## EXPERIMENT METHODOLOGY

$\text{K}_2\text{Cr}_3\text{As}_3$  was synthesized as described in Ref. 1. For total scattering experiments on the NOMAD diffractometer  $\sim 2$  g of material was loaded into a 6 mm diameter vanadium PACS can. All sample handling was performed in a high purity He glovebox to protect the sample from exposure to air. Measurements were carried out in a cryostat over the temperature range  $2\text{K} \leq T \leq 300\text{K}$ . Data were collected at 2, 50, 150, 200 and 300 K and in 2 K steps between 2 and 20 K with collection times of 4 hrs and 30 mins respectively. Scans of an empty 6 mm vanadium PACS can were collected in a cryostat for background correction with 3 hrs of count time. All scans were performed on warming.

The resulting diffraction patterns were transformed into  $G(r)$  using the fastgr software [2]. It is an inescapable limitation of physical diffractometers that only a finite range of usable  $Q$ 's can be collected in part due to: limitations of scattering geometry, finite sample size and scattering properties of the sample. In the Fourier transform of  $S(Q)$  to  $G(r)$  this results two completing concerns when deciding were to truncate the transform (e.g. at what  $Q_{max}$ ). The larger the range of  $Q$  used in the transformation the higher the resolution of the resulting  $G(r)$  however, as higher  $Q$  is including the strength of the sample scattering decreases and noise becomes more prominent approaching and surpassing the size of the sample signal (Fig. S1) [3]. This noise present at high  $Q$  when transformed leads to large artificial ripples in  $G(r)$  which can contaminate analysis [3].

In order to check for such artifacts, we performed data reduction with varying  $Q_{max}$  values. The resulting  $G(r)$  for  $Q_{max} = 25, 28, \text{ and } 31 \text{ \AA}^{-1}$  are shown in Fig. S1 with an arbitrary vertical offset. One way to characterize these artifacts is via the magnitude, width and peak position dependence on  $Q_{max}$  of the low- $r$  oscillations seen below the lowest known bond (i.e.  $\sim 2.3 \text{ \AA}$ ). In our patterns these features are smaller than our considered signal and show a significant position dependence on  $Q_{max}$ . As a further check, analysis of fits using the  $P\bar{6}m2$  and  $Amm2$  models discussed in the main text were performed for the three  $G(r)$ 's and, in each fit, produced similar results.

For our final PDF analysis, a  $Q_{max}$  of  $31 \text{ \AA}^{-1}$  was used for  $T < 200 \text{ K}$ . For higher temperature data, where larger thermal vibrations lead to a quicker drop off in the structure factor, a  $Q_{max}$  of  $28 \text{ \AA}^{-1}$  was used.

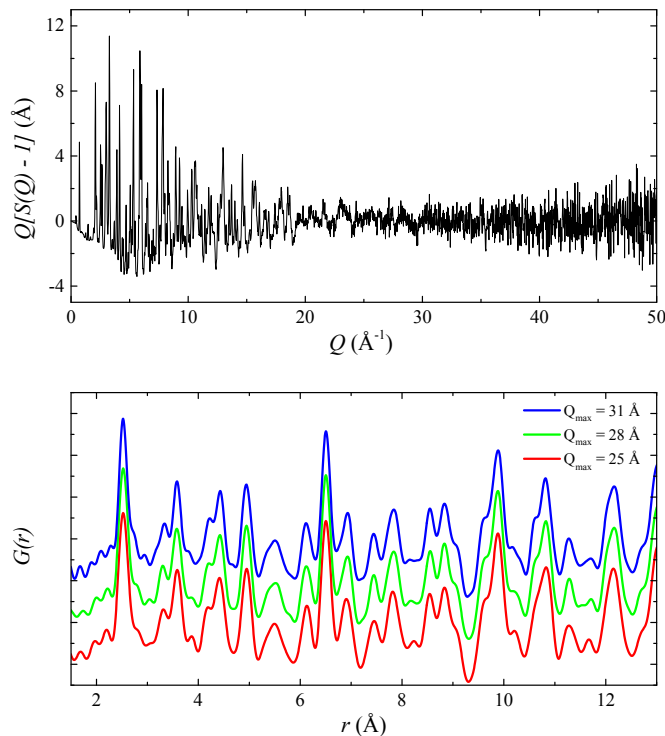


FIG. S1. Normalized and  $Q$  scaled total scattering structure factor  $Q[S(Q) - 1]$  (top). Radial distribution function  $G(r)$  for  $Q_{max} = 25, 28, \text{ and } 31 \text{ \AA}^{-1}$  showing artifacts due to termination ripples and noise (bottom).



### $I(Q)$ REFINEMENTS

Rietveld refinements using the standard diffraction data technique were performed using the GSAS and EXPGUI software suites [4, 5]. The time-of-flight profile function TYPE-3 of GSAS was used to model the peak profile via convoluted back-to-back exponentials convoluted with a pseudo-Voigt [6]. All data was well fit by a single phase using the average  $P\bar{6}m2$  space group of  $K_2Cr_3As_3$ . A fit to the 2 K data is shown in Fig. S2 with goodness of fit parameters  $\chi^2 = 13.88$ ,  $R_p = 6.7\%$  and  $R_{wp} = 6.7\%$ . Similar fits were obtained for all temperatures.

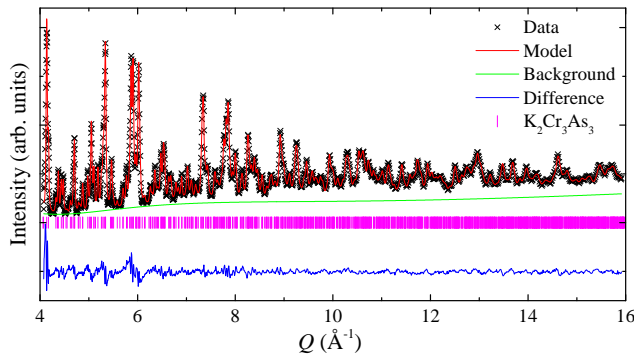


FIG. S2. Rietveld fit of  $P\bar{6}m2$  model using the 2 K data collected by BANK 5 of the NOMAD diffractometer

## PAIR DISTRIBUTION FUNCTION REFINEMENTS

Small box modeling of the pair distribution function  $G(r)$  was performed using the PDFgui software [3, 7]. The instrumental terms  $Q_{damp}$  and  $Q_{broad}$  were determined by refinements using data collected on the instrument standards (silicone and diamond powders) in an Orange cryostat and fixed for all modeling of the  $\text{K}_2\text{Cr}_3\text{As}_3$  data. Figure. S3 shows a best fit using the  $P\bar{6}m2$  symmetry of the 2 K Fourier transformed NOMAD data over the range  $0.1 \text{ \AA} \leq r \leq 35 \text{ \AA}$  with fit parameters of  $\chi^2 = 0.1$  and  $R_w = 16\%$ . As seen the model has difficulties reproducing both the low and high  $r$  data leading to the poor fit parameters (we note that the goodness of fit parameters for the standards in the cryostat were  $\chi^2 \sim 1.5$  and  $R_w \sim 11\%$  (for the same  $r$ -range) indicating the baseline for quality of fit).

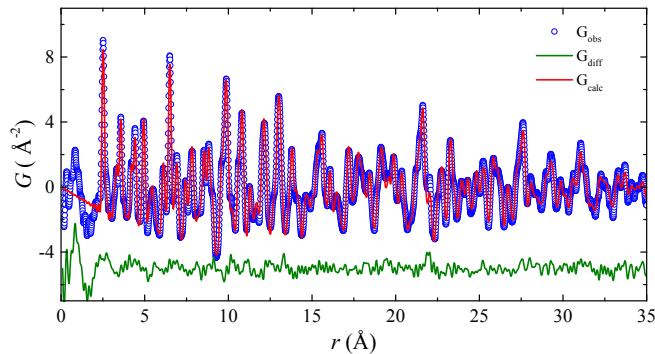


FIG. S3. PDFgui fit to  $G(r)$  collected on NOMAD at 2 K using the  $P\bar{6}m2$  model.

Figure S5 shows a comparison of the low- $r$  PDFgui fits using the  $P\bar{6}m2$  and  $Amm2$  models and the constituent partial  $G(r)$ 's ( $G_p(r)$ ). These models were fit using the same number of refinable parameters to allow for an unambiguous assessment of each model's validity. In the case of  $P\bar{6}m2$ , the starting crystallographic structure was expanded using the space group symmetry elements leading to a total of 16 atomic sites. Constraints were placed on the atomic positions and anisotropic ADP's such that the original symmetry operations were still enforced in the small box model. In addition to these parameters, a scale factor was refined and a term to account for correlated motion (see Ref. 7).

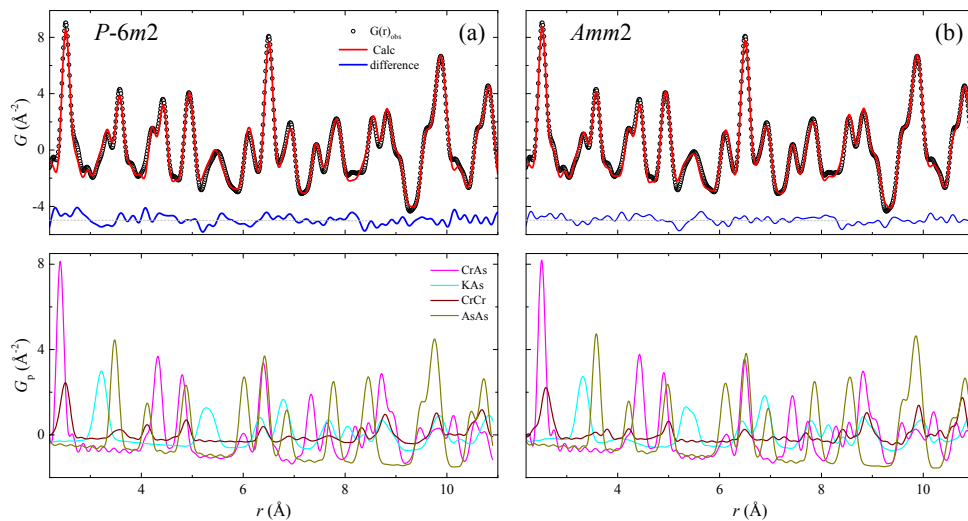


FIG. S4. PDFgui fits to 2 K  $G(r)$  patterns comparing the  $P\bar{6}m2$  (a) and  $Amm2$  (b) models. The lower panels show the partial  $G(r)$ 's for the Cr-As, K-As, Cr-Cr and As-As correlations.

The orthorhombic  $Amm2$  model (see later sections for details of the distortion) results in an expansion of the unit to the new basis  $(0, 0, -1), (0, 1, 0), (2, 1, 0)$  in terms of the original lattice parameters  $(a, a, c)$  and an increase in the number of symmetry independent atomic sites from 6 to 11. The lowering in symmetry from hexagonal to

orthorhombic and the increased number of atomic sites creates additional refinable parameters in both the lattice parameters and the atomic positions. To account for this in our refinements, we constrained the orthorhombic  $a$  and  $c$  lattice parameters by a scale factor and refined the ADP's as isotropic. Furthermore, we constrained the ADP's for each atomic species to be equivalent (e.g. all As ADP's were refined by a single parameter). In doing so, the  $P\bar{6}m2$  model and the constrained  $Amm2$  model were refined using the same number of parameters. We note that refinements of the  $Amm2$  model were also performed without such constraints, the resulting fit produced lower goodness-of-fit parameters but qualitatively similar conclusions. We therefore, feel justified that the constraints are not artificially influencing the reported local structure.

As discussed in the main text, the widely reported  $P\bar{6}m2$  model fits poorly in the low  $r$  range - missing shoulders at  $\sim 2.6$ , and  $5.4$  Å and systematically under/over-fitting adjacent peaks particularly of K-As character. Comparing the partial  $G(r)$  in panels  $a$  and  $b$  of Fig. S5, it is seen that the  $Amm2$  model is able to account for this by creating a new series of Cr-As and K-As bond lengths - splitting the peak at  $5.4$  Å (which is almost entirely K-As in character) and splitting the Cr-Cr peak at  $\sim 2.5$  Å. In fact, the  $G_p(r)$  of As-As barely changes between the two. We attribute this distortion mainly to a displacement of the K2 site which consequently redistributes electron density in the Cr-Cr plaquettes (see main text).

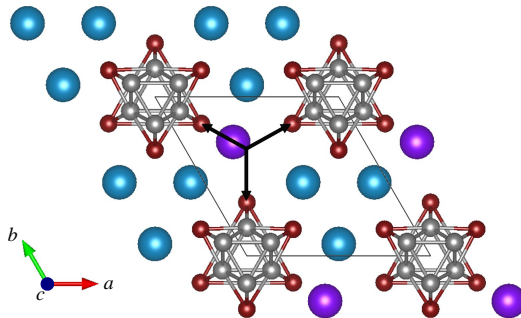


FIG. S5. Structure of  $P\bar{6}m2$  symmetry model refined with no constraints on in-plane K2 position. Black arrows added to indicate three equivalent displacement directions from crystallographic K2 site to neighboring CrAs tubes. The Cr, As, K1 and K2 sites are indicated by gray, red, teal and purple spheres respectively.

To check this interpretation, refinements were performed with the  $P\bar{6}m2$  model but with the in-plane symmetry constraints of the K2 site's Wyckoff position removed (*i.e.*  $(x, y, z) = (\frac{1}{3}, \frac{2}{3}, 0)$ ). In contrast to the  $Amm2$  model whose symmetry only allows K2 displacements along the  $(2, 1, 0)$  direction (in the original lattice setting), here the K2 is loosed to move any in-plane direction in-plane. Refinements of this model result in reduced goodness-of-fit parameters (from  $R_w \sim 14\%$  to  $13\%$ ) and a significant reduction of the K2 site's in-plane ADP's (by an order of magnitude from  $\sim 0.1$  to  $0.01$  Å<sup>2</sup>). Considering the refined K2 position, it distorts from the special site to  $(0.28, 0.71, 0)$  - along the line connecting the K2 and the CrAs tube center, in agreement with the  $Amm2$  refinements.

In addition to the  $k = (0, 0, 0)$   $Amm2$  model as a simple check, small box modeling was also attempted using  $k = (\frac{1}{2}, 0, 0)$ ,  $(\frac{1}{2}, \frac{1}{2}, 0)$  and  $(0, 0, \frac{1}{2})$  distortions. We note that overall, these lower-symmetry models result in many additional refinable parameters. Especially considering the limited  $r$  ranges used in our analysis, we treated additional refinable parameters with suspicion out of concern for artificially decreasing goodness-of-fit measures from increased model parameters and questions of over-fitting. Therefore, despite marginally better fits being achieved with distortions allowed by both attempted in-plane ordering vectors, we focus on the  $Amm2$  model for its relative simplicity, the organic indication of a  $(2, 1, 0)$  displacement direction from the refinements described above and the results of our DFT calculations. On the other hand, models generated from the out of plane  $(0, 0, \frac{1}{2})$  distortion direction were unable to improve our fit and were generally unstable as atoms were displaced from the  $z = 0, \frac{1}{2}$  planes. This is unsurprising considering the results of our anisotropic ADP analysis which strongly indicate the distortion to be in-plane.

**DISTORTIONS TO THE  $P\bar{6}m2$  STRUCTURE**

The results of our DFT calculations, ADP analysis and PDF refinements in the  $P\bar{6}m2$  model with loosed K2 positions indicate the structural distortion to be in the  $ab$  plane and likely along the K2 - Cr2 vector. Furthermore, the energy minimization work suggests a  $Amm2$  orthorhombic distortion. Using these results as a starting point we performed Group Theory analysis of distortions to the  $P\bar{6}m2$  symmetry to further characterize the distortion.

TABLE S1. Irreducible representations ( $\Gamma$ ), order parameter, space group and basis vectors for orderings with  $k = (0, 0, 0)$

$\Gamma$	Order parameter	Space group	Basis
$GM_1(k16t1)$	$(a)$	$P\bar{6}m2$	$(1, 0, 0), (0, 1, 0), (0, 0, 1)$
$GM_2(k16t3)$	$(a)$	$P\bar{6}$	$(1, 0, 0), (0, 1, 0), (0, 0, 1)$
$GM_3(k16t4)$	$(a)$	$P3m1$	$(1, 0, 0), (0, 1, 0), (0, 0, 1)$
$GM_5(k16t5)$	$(a, -1.732a)$	$Amm2$	$(0, 0, -1), (0, 1, 0), (2, 1, 0)$
	$(a, b)$	$Pm$	$(0, 1, 0), (0, 0, 1), (1, 0, 0)$
$GM_6(k16t6)$	$(a, -1.732a)$	$C2$	$(0, -1, 0), (2, 1, 0), (0, 0, 1)$
	$(a, 0.577a)$	$Cm$	$(2, 1, 0), (0, -1, 0), (0, 0, -1)$
	$(a, b)$	$P1$	$(0, 0, 1), (1, 0, 0), (0, 1, 0)$

Table S1 shows  $k = (0, 0, 0)$  allowed distortions. The corresponding irreducible representations (irreps  $\Gamma$ ), order parameters, space groups and basis vectors were determined using the ISODISTORT program [8]. The  $k = (0, 0, 0)$  produces five irreps and eight possible distorted structures. The first three irreps ( $GM_1$ ,  $GM_2$  and  $GM_3$ ) maintain a screw/inversion symmetry element along the  $c$ -lattice direction and so disallow in-plane displacements of the K2 site. The first irrep/order parameter combination to allow such a displacement is  $GM_5/(a, -1.732a)$  which results a new orthorhombic basis set and the  $Amm2$  space group. The  $E'(a)$  mode of  $GM_5$  causes a displacement of the K2 site along the order parameter direction - along the  $(2,1,0)$  direction or  $c$ -axis of the orthorhombic cell. This distortion is consistent with our PDF modeling in  $P\bar{6}m2$  with the in-plane symmetry constraints of K2 removed. As the highest symmetry model consistent with our previous modeling and with a symmetry predicted by our DFT work, we used the  $Amm2$  symmetry for our small box modeling of the distortion.

We note that while lower symmetry distortions with  $k = (0, 0, 0)$  or with other in-plane ordering vectors also allowed such a distortion, they also resulted in a significant increase in the number of refinable parameters (see previous section) and therefore only report on the  $Amm2$  model.

## DETAILS OF DENSITY FUNCTIONAL THEORY CALCULATIONS

Density functional calculations were performed using the Perdew-Burke-Ernzerhof generalized gradient approximation (PBE-GGA)[9]. The lattice parameters were fixed at the experimental values, and all free internal atomic positions were relaxed subject to the hexagonal symmetry. As discussed, our results strongly differ from the previously reported stable phonons of Subedi. Accordingly, we did extensive convergence tests and employed two different electronic structure methods, specifically the projector-augmented wave method, as implemented in the VASP code Refs. 10 and 11 and the general potential linearized augmented planewave method as implemented in WIEN2k Ref. 12. We carefully tested different convergence criteria, especially Brillouin zone samplings and basis set cut-offs in the VASP calculations. The phonons were obtained using the supercell finite difference method based on VASP calculations using the PHONOPY code [13]. For this we tested different supercells. The result shown is for a  $2 \times 2 \times 3$  supercell containing 192 atoms. As shown we find a strong phonon instability throughout the  $k_z = 0$  plane. We relaxed the structure, again using VASP, keeping the lattice parameters fixed, without imposing hexagonal symmetry and found a lower symmetry orthorhombic  $Amm2$  structure. We did a similar relaxation using WIEN2k and also find that the hexagonal structure is unstable, and that the  $Amm2$  structure is lower in energy similar to the VASP result. The calculated energy lowering is 17 meV per formula unit.

---

\* corresponding author taddeikm@ornl.gov

† corresponding author singhdj@missouri.edu

- [1] K. M. Taddei, Q. Zheng, A. S. Sefat, and C. de la Cruz, *Phys. Rev. B* **96**, 180506 (2017).
- [2] M. T. McDonnell, D. P. Olds, K. L. Page, J. C. Neufeind, M. G. Tucker, J. C. Bilheux, W. Zhou, and P. F. Peterson, *Acta Crystallographica Section A* **73**, a377 (2017).
- [3] T. Proffen and S. J. L. Billinge, *Journal of Applied Crystallography* **32**, 572.
- [4] B. H. Toby, *Powder Diffraction* **21**, 67 (2006).
- [5] J. Larsen, B. M. Uranga, G. Stieper, S. L. Holm, C. Bernhard, T. Wolf, K. Lefmann, B. M. Andersen, and C. Niedermayer, *Physical Review B* **91**, 024504 (2015).
- [6] R. B. Von Dreele, J. D. Jorgensen, and C. G. Windsor, *Journal of Applied Crystallography* **15**, 581 (1982).
- [7] C. Farrow, P. Juhas, J. Liu, D. Bryndin, E. Boin, J. Bloch, T. Proffen, and S. Billinge, *Journal of Physics: Condensed Matter* **19**, 335219 (2007).
- [8] B. J. Campbell, H. T. Stokes, D. E. Tanner, and D. M. Hatch, *Journal of Applied Crystallography* **39**, 607 (2006).
- [9] J. P. Perdew, K. Burke, and M. Ernzerhof, *Phys. Rev. Lett.* **77**, 3865 (1996).
- [10] G. Kresse and D. Joubert, *Phys. Rev. B* **59**, 1758 (1999).
- [11] G. Kresse and J. Furthmüller, *Phys. Rev. B* **54**, 11169 (1996).
- [12] D. Singh and L. Nordström, *Planewaves, Pseudopotentials and the LAPW Method*, 2<sup>nd</sup> ed. ed. (Springer, Berlin, 2006).
- [13] A. Togo and I. Tanaka, *Scripta Materialia* **108**, 1 (2015).